https://doi.org/10.5194/egusphere-2026-3089
Preprint. Discussion started: 11 June 2026

Urban surface-atmosphere fluxes of pptv-level oxygenated organic molecules (OOMs) from eddy covariance observations

Jieya Sun[1], Xinyu Wang[1], Jingya Hua[1], Bo Zhu[2], Nan Chen[2], Huan Yu[1*]

1. Department of Atmospheric Science, School of Environmental Studies, China University of Geosciences, Wuhan 430074, China
2. Hubei Ecological Environment Monitoring Center Station, Wuhan 430070, China

Correspondence: Huan Yu, yuhuan@cug.edu.cn

Abstract

Oxygenated Organic Molecules (OOMs) represent a substantial fraction of ambient reactive carbon and are potential precursors of secondary organic aerosols (SOA). Surface-atmosphere exchange flux modulates OOM budgets and subsequent SOA formation. This study presents the first urban eddy covariance measurements of pptv-level OOM surface-atmosphere fluxes, using an iodide-adduct chemical ionization mass spectrometer during the hottest month of the year in a central China megacity. We addressed the challenges of retrieving reliable fluxes for OOM species with low concentration signal-to-noise-ratios. Effects of data block averaging and water vapor dilution were investigated. We retrieved the fluxes of 16 OOMs, which displayed highly variable exchange behavior and fell into three categories: deposition-dominated, emission-dominated, and bidirectional exchange. Campaign-averaged total daily OOM deposition flux 1.64 μmol m^{-2} d^{-1} was 16.3% of HNO_3 deposition flux, but 4 times larger than the total daily OOM emission flux. Isoprene-derived organonitrate $C_4H_7NO_5$, IEPOX+ISOPOOH ($C_5H_{10}O_3$), formic acid, and nitrophenol $C_6H_5NO_3$ are identified as the dominant contributors to the total OOM fluxes. OOM fluxes at this urban site, however, were one to two orders of magnitude lower than previous flux observations above forest canopy. This work provides key methodological guidance and observational constraints for surface-atmosphere exchange of underrepresented reactive carbons.

https://doi.org/10.5194/egusphere-2026-3089
Preprint. Discussion started: 11 June 2026

1 Introduction

Oxygenated Organic Molecules (OOMs) are a group of low-volatility organic compounds typically containing 2-7 oxygen atoms. OOMs represent a substantial fraction of ambient reactive carbon and are potential precursors to secondary organic aerosols (SOA). Beyond atmospheric production and removal reactions, OOM budget in the atmosphere is modulated by complex surface-atmosphere exchange processes including surface emissions and dry deposition (Ehn et al., 2014; Fulgham et al., 2019). Currently, chemical transport models (CTMs) incorporate dry deposition schemes for only a very limited number of OOM, with deposition velocities poorly parameterized due to the lack of accurate effective Henry's law constants and surface reactivity data (Hodzic et al., 2013; Kelly et al., 2019; Wu et al., 2021; Zhang et al., 2003). This challenges accurate OOM budget estimates.

Direct OOM flux measurements, either emission or deposition, are essential for quantifying the atmospheric reactive carbon budget and constraining CTM predictions. The eddy covariance (EC) technique, the most accurate in-situ flux method, quantifies turbulent fluxes by measuring the covariance of vertical wind and concentration fluctuations. Many studies employed the EC technique coupled with proton-transfer-reaction mass spectrometry (PTR-MS) to measure VOC fluxes, primarily focusing on hydrocarbons (Fischer et al., 2021; Kim et al., 2017; Manco et al., 2022; Ruuskanen et al., 2011; Valach et al., 2015; Velasco et al., 2009; Vettikkat et al., 2023; Yuan et al., 2015; Zavarsky et al., 2018) and oxygenated VOCs (e.g., alcohols, aldehydes, and ketones; (Acton et al., 2020; Bachy et al., 2020; DiGangi et al., 2011; He et al., 2026; Hörtnagl et al., 2011; Karl et al., 2018). However, PTR-MS does not detect OOMs (e.g., organic acids, organonitrates, organosulfur compounds, hydroperoxides) that typically undergo bidirectional surface-atmosphere exchange.

Field-deployable negative-ion chemical ionization mass spectrometry (CIMS) (e.g., using I^-, CH_3COO^-, CF_3O^- ions) can detect OOMs, thereby enabling OOM flux measurement (Beaver et al., 2012; Bertram et al., 2011; Lee et al., 2014; Mattila et al., 2018). Despite these advances, most of existing studies focused only on formic acid

https://doi.org/10.5194/egusphere-2026-3089
Preprint. Discussion started: 11 June 2026

(Fulgham et al., 2019; Gao et al., 2022; Nguyen et al., 2015; Schobesberger et al., 2016; Vermeuel et al., 2023) and peroxyacyl nitrates (PANs) (Min et al., 2012; Phillips et al., 2013; Turnipseed et al., 2006; Wolfe et al., 2009). Full-spectrum OOM flux measurements remain limited, and have been mostly conducted above forest canopies (Fulgham et al., 2019; Nguyen et al., 2015; Vermeuel et al., 2023).

Virtually no OOM flux measurements have been reported for urban environments, where governing factors of OOM fluxes (natural/anthropogenic emissions, near-surface chemical production and loss, and deposition resistance towards heterogeneous urban surfaces) are highly complex. Here, we deployed an iodide-adduct CIMS (I-CIMS) coupled with EC to measure surface-atmosphere fluxes of OOMs in an urban environment during the hottest month of a year. Unlike ppbv-level VOCs, OOMs typically occur at pptv or lower concentrations, and thus pose more measurement challenges (Langford et al., 2015). We specifically investigated optimized flux processing methods for the OOM with low signal-to-noise ratio (SNR) in their concentration measurements.

2 Methodology

2.1 Site Description and Eddy Covariance Measurements

Field measurements were conducted from July 14 to August 10, 2025 at a municipal air quality monitoring supersite on a university campus (114.6157°E, 30.4577°N) in Wuhan, a central Chinese inland megacity. A three-dimensional sonic anemometer (Campbell Scientific, CSAT3B) and an I-CIMS sampling inlet were mounted on a 10 m cylindrical mast atop the 20-m-high supersite building. The site is surrounded by wooded areas in the southwest and northeast, and a mixed building-tree campus landscape in other directions, with surrounding buildings averaging 15 m in height. Northeast winds prevailed throughout the campaign. Flux footprint analysis (Figure S1) indicates that 90% of the measured fluxes originated from within 500 m of the supersite. The campaign covered the annual peak of temperature, humidity and solar radiation; short rainfall events were excluded from flux analysis. The site was characterized by strong summertime biogenic emissions from vegetation overlapped with potential

https://doi.org/10.5194/egusphere-2026-3089
Preprint. Discussion started: 11 June 2026

urban anthropogenic sources.

The horizontally mounted, west-facing sonic anemometer recorded 3D wind components and sonic temperature (T_s) at 10 Hz, with negligible flow distortion from the slender mast. The I-CIMS inlet was set 0.23 m below and 0.85 m east of the sonic sensor to minimize sensor separation. Following Fulgham et al. (2019) and Vermeuel et al. (2023), who used long PFA/FEP tubes to sample atmospheric OOMs from flux tower tops, we drew ambient air through a 20.8-m-long, 3/8-inch ID PFA tube at 80 standard liters per minute (SLPM, calculated to be in the turbulent flow regime) to the I-CIMS housed in an air-conditioned room on the building's top floor. A schematic of the observation system is provided in Figure S2. The indoor segment of the PFA tube was heated to 40 °C to minimize wall interactions and water vapor condensation. Reversible adsorption/desorption of OOMs on PFA tubing surfaces were documented (Liu et al., 2019; Nguyen et al., 2015), which preserves bulk concentration but introduces high-frequency flux attenuation. Low-pass spectral correction (Ibrom et al., 2007) was adopted to correct high-frequency flux loss (discussed in section 3.1).s

The I-CIMS operated at 1.8 SLPM to measure iodide adducts of OOMs and inorganic species (e.g., HNO_3) at 10 Hz. A 36-minute measurement cycle was applied, including 31 min for ambient sampling and 5 min for high-purity nitrogen blank correction. Air temperature and relative humidity were monitored at 1 Hz at the inlet of I-CIMS. Sonic and I-CIMS datasets were independently collected with unified time synchronization. After strict quality control, valid data of 28 days were used for flux analysis.

2.2 I-CIMS data processing

2.2.1 Peak fitting of target OOMs

After mass calibration and peak fitting of raw mass spectra, exact peak masses were matched to plausible chemical formulas $C_{1\text{-}30}H_{1\text{-}60}O_{0\text{-}20}N_{0\text{-}2}S_{0\text{-}2}I_{0\text{-}1}^-$ under elemental ratio constraints. Mass assignment was performed with a mass error <10 ppm at MS resolution of ~6000. Priority was given to elemental formulas corresponding to atmospherically relevant OOM species reported by previous studies. This workflow identified over 400 ion formulas, whose 10 Hz time series were normalized to one

https://doi.org/10.5194/egusphere-2026-3089
Preprint. Discussion started: 11 June 2026

million reagent ions (total I^- and IH_2O^-) (Text S1).

The SNRs for the 10 Hz ion signals were calculated over 30-minute intervals and averaged to obtain mean SNRs for 0.1-second integration time. Only iodide-adduct ions with mean SNR > 2 were retained as target ions; this threshold corresponds to an SNR > 18 for 1-minute integration time, which was commonly reported in concentration measurements. The retained ions were therefore also those with the high signal intensities. The target ions suffering from severe interference by adjacent peaks were also discarded. In total, 21 target OOMs, in the form of iodide-adduct ions shown in Table S1, were selected for a second run of peak fitting to produce refined 10 Hz time series, which were used for flux calculation.

2.2.2 Calibration of OOM Mixing Ratios

Authentic standards are unavailable for most OOM species detected by the I-CIMS, making compound-specific calibration infeasible. In this study, OOM response factors were quantified via a collision-limited sensitivity calibration method (Isaacman-VanWertz et al., 2018; Lopez-Hilfiker et al., 2016) from three components: (1) maximum instrumental sensitivity (S_{max}), referring to the sensitivity of compounds forming $M{\cdot}I^-$ adducts at collision limit, (2) the relative sensitivity of $M{\cdot}I^-$ adducts ($1/S_0$) due to partial declustering in the electric fields, and (3) mass-dependent transmission efficiency (T_M) of $M{\cdot}I^-$ adducts relative to I^- reagent ion within ion optics and detector. The full workflow for determining response factor ($S_{\max} \times 1/S_0 \times T_M$, units: cps $pptv^{-1}$) is presented in Text S2-S4. S_{max} was calibrated using levoglucosan, a reference compound forming $M{\cdot}I^-$ adduct at collision limit. Direct calibration factors of HNO_3 and formic acid, both of which have commercially available certified permeation tubes, were measured to validate the approach. All target OOM response factors are listed in Table S1. The overall calibration uncertainty of this method is estimated to be 33–65% (2σ, 95% confidence interval), varying with the target species (Text S5).

2.3 Eddy Covariance Data Processing and Quality Control

Under the assumptions of negligible horizontal and vertical advection, the EC flux F is defined as:

https://doi.org/10.5194/egusphere-2026-3089
Preprint. Discussion started: 11 June 2026

$$F = \rho_d \overline{w'c'} \quad (1)$$

where ρ_d is the dry air density, w' is the fluctuation in vertical wind speed, and c' is the fluctuation in OOM dry mole fraction. Prior to eddy covariance flux calculations, all 10 Hz raw data (wind components, T_s, c) were standardized preprocessed using EddyPro 7.0 software, including geographic yaw correction, double rotation for tilt/terrain bias removal, and Vickers and Mahrt (1997) quality control (despiking + statistical screening). Invalid 30-minute intervals with failed critical variable flags were excluded (Text S6).

To correct tube transport delay in the closed-path system, actual lag times between gas concentrations and vertical wind speed were determined using the maximum cross-covariance method (Text S7). In practice, the signals of some low-SNR OOM may cause noise-induced mismatches between 10 Hz concentration and wind speed data, introducing uncertainties in species-specific lag time derivation. Following Fares et al. (2012), we assumed identical turbulent transport for all species passing through the same sampling tube. HNO_3, with the highest SNR, was selected as the reference tracer, and its 30-minute lag times were uniformly applied to all OOMs. This approach reduced random errors for low-SNR OOMs and improved time alignment accuracy for flux calculations. The HNO_3 lag times exhibited a mean diurnal value of 1.72 ± 0.88 s (Figure S5).

After lag time correction, a 250 s moving average detrending was applied to the 10 Hz raw data for each 30-minute interval to remove low-frequency non-turbulent trends from diurnal cycles, synoptic weather processes, and background signal fluctuations. Raw fluxes were then calculated per Equation 1.

All half-hourly fluxes were quality-screened via the steady state test (SST) and integral turbulence characteristic (ITC) test per Foken et al. (2004). These tests assess covariance stationarity across sub-intervals within 30-minute and agreement between measured dimensionless concentration variances and Monin-Obukhov similarity theory (MOST) predictions, respectively, producing quality flags (Text S8). Fluxes failing these tests were excluded from further analysis.

https://doi.org/10.5194/egusphere-2026-3089
Preprint. Discussion started: 11 June 2026

Friction velocity (u^*) and Monin-Obukhov stability parameter (z/L) were also used to assess data quality. Over the campaign, 86% of the half-hourly u^* values exceeded 0.2 m s^{-1}, indicating well-developed turbulent mixing. z/L ranged from -2 (strongly unstable) to slightly positive values (weakly stable).

Random sampling uncertainty in 30-minute eddy covariance fluxes, arising from stochastic turbulence sampling and instrument noises, was quantified using the method of Finkelstein and Sims (2001) (Text S9). The method is based on the variance of a covariance between vertical wind velocity and scalar concentration, which are auto- and cross-correlated. The resulting standard error σ_F defines a ~68% confidence interval ($F \pm \sigma_F$) around each flux estimate. Flux detection limits, set at $3\sigma_F$ for all species, are provided in Table S1.

3. Results and discussion

3.1 Spectral analysis and flux loss correction

Spectral analysis is critical for assessing turbulence data quality, validating flux consistency, and diagnosing system high-frequency response limitations. The mean SNRs of the 10 Hz ion signals for the target OOMs range from 2.1 to 9.9 in the campaign, corresponding to 19–63 at 1-minute integration time. Such low SNRs at 0.1 s integration time were also reported by prior EC flux studies of OOM or OVOCs (Coggon et al., 2021; Nguyen et al., 2015; Yang et al., 2013). To examine how spectral behavior varies with SNR, we selected four representative species spanning the observed SNR range: high-SNR HNO_3 (9.9), medium-SNR $C_4H_7NO_5$ (5.6) and CH_2O_2 (3.6), and low-SNR $C_3H_4O_4$ (2.2), all at 0.1 s integration time. Power spectra (w, T_s, HNO_3/OOMs) and cospectra (w-T_s, w-HNO_3/OOM) were computed via Fast Fourier Transform from 30-minute fluctuation time series and averaged into logarithmically spaced frequency bins.

Variance-normalized mean power spectral densities (PSDs) for 12:00–15:00 local time show that the T_s spectrum follows the theoretical Kolmogorov −5/3 slope in the inertial subrange (frequency > 0.002 Hz in this study), confirming adequate sonic anemometer response and well-developed turbulence (Figure 1a). In contrast, HNO_3

https://doi.org/10.5194/egusphere-2026-3089
Preprint. Discussion started: 11 June 2026

and OOM PSDs deviate significantly from T_s. For species with SNR > 2.2, spectra flatten above ~0.1 Hz as instrumental white noise dominates. For $C_3H_4O_4$ (SNR = 2.2), the spectrum is nearly flat across all frequencies with no discernible slope, indicating complete noise domination. This precludes reliable flux characterization, as corroborated by $C_3H_4O_4$'s near-zero uncorrected raw fluxes (Figure S6). All OOM species with SNR ≤ 2.2 were therefore excluded from subsequent flux calculations.

To assess noise impacts on flux recovery, we further examined normalized cumulative cospectra (ogives) for the selected species (Figure 1b), which quantify the cumulative flux contribution of turbulent eddies at each frequency. The T_s ogive serves as a near-ideal unattenuated reference and decays smoothly from 1 to 0 across 0.001–2 Hz, confirming the sonic anemometer captures all relevant turbulent scales. For HNO_3 and OOMs, most flux originates from eddies below 0.1 Hz; above 0.1 Hz, ogives fluctuate around zero, indicating random noise dominates and contributes negligibly to net flux. We corrected this noise before high-frequency loss correction: the high-frequency noise floor was estimated from the flat plateau in HNO_3/OOM power spectra (Figure 1a), extrapolated to lower frequencies, and subtracted from raw spectra. Noise-corrected spectra (Figure 1c) exhibit decay behavior similar to T_s, confirming physically realistic turbulent behavior.

In the frequency domain, the measurement system attenuates turbulent fluctuations, causing flux underestimation. Flux loss arises from two sources: (1) low-frequency attenuation due to the 30-minute averaging interval and detrending; and (2) high-frequency attenuation from instrument response, path averaging, sensor separation, and inlet tube smearing. High-frequency attenuation is evident in Figure 1c, where noise-corrected spectra of all species decay steeper than T_s, indicating damping of small-scale eddies.

Low-frequency flux correction was performed using the analytical method of J. Moncrieff et al. (2004), yielding a single correction factor for all target species per 30-minute interval. The mean high-pass spectral correction factor (HPSCF) was 1.13 ± 0.07, corresponding to an average low-frequency flux loss of 11.5% ± 5.3% (Text S10).

https://doi.org/10.5194/egusphere-2026-3089
Preprint. Discussion started: 11 June 2026

While the theoretical approach of J. B. Moncrieff et al. (1997) can also be used for high-frequency correction, it requires accurate system response time characterization, which is not feasible here due to species-dependent wall adsorption-desorption in the long PFA inlet. High-frequency correction was therefore performed using the empirical field-based method of Ibrom et al. (2007), which compares the unattenuated T_s power spectrum with denoised HNO_3/OOM spectra to yield compound-specific correction factors (Text S11). Mean low-pass spectral correction factors (LPSCF) were 1.12 ± 0.05 for HNO_3, 1.49 ± 0.23 for $C_4H_7NO_5$, and 1.22 ± 0.11 for CH_2O_2, corresponding to average high-frequency flux losses of 10.9% ± 3.9%, 31.5% ± 9.8%, and 17.6% ± 6.6%, respectively (Table 1).

Combining low- and high-frequency corrections yields total spectral correction factors (SCF). For HNO_3, the mean SCF was 1.27 ± 0.05, corresponding to mean total flux loss of 21.1% ± 2.8%. Due to species-specific response times and inlet wall interactions, $C_4H_7NO_5$ and CH_2O_2 exhibited larger SCFs and total flux losses than HNO_3 (Table 1). SCF values for remaining species are listed in Table S1.

3.2 The effects of CIMS sampling frequency and Water Vapor Dilution

3.2.1 The effects of sampling frequency on flux

Because 10 Hz CIMS sampling introduces significant high-frequency noise, we tested whether block-averaging 10 Hz data to 1 Hz suppresses noise and improves flux estimates. Figure 1d compares 10 Hz and 1 Hz fluxes, both raw and spectra-corrected, revealing three key findings: (1) Fluxes from 1 Hz and 10 Hz data are strongly correlated ($R^2 > 0.9$, $p<0.05$) for all three species. (2) For HNO_3, 1 Hz raw fluxes are on average 12% lower than 10 Hz raw fluxes; this difference increases to 15% after spectral correction, as 1 Hz sampling misses flux contributions from 0.5 - 5 Hz. (3) For $C_4H_7NO_5$ and CH_2O_2, raw fluxes differ by <1% between 1 Hz and 10 Hz, as their spectra are noise-dominated in the 0.5 - 5 Hz range with negligible flux contributions. After high-frequency correction, however, 1 Hz corrected fluxes exceed 10 Hz values, driven by larger SCFs for 1 Hz data: 1.78 ± 0.22 (10 Hz) *vs.* 1.88 ± 0.26 (1 Hz) for $C_4H_7NO_5$; 1.53 ± 0.12 (10 Hz) *vs.* 2.09 ± 0.35 (1 Hz) for CH_2O_2. This discrepancy arises

https://doi.org/10.5194/egusphere-2026-3089
Preprint. Discussion started: 11 June 2026

from differences in high-frequency noise removal: for 1 Hz data, power spectral density at $f > 0.2$ Hz was treated as noise, while for 10 Hz data the noise floor was determined at $f > 2$ Hz. Overestimation of the high-frequency noise level in 1 Hz spectra leads to an artificially low cutoff frequency (f_c), which in turn produces inflated LPSCFs.

In summary, reducing sampling frequency improves SNR but introduces systematic flux biases: underestimation for high-SNR species (e.g., HNO_3) and overestimation for medium-SNR species (e.g., $C_4H_7NO_5$ and CH_2O_2), stemming from errors in noise removal and high-frequency correction. All subsequent analyses therefore used the 10 Hz dataset.

3.2.2 Assessment of Water Vapor Dilution Effects

The eddy covariance method quantifies trace gas fluxes arising from the net addition or removal of gases via emission or deposition, rather than from apparent concentration changes induced by air temperature or water vapor content variations. In this study, the CIMS inlet was equipped with long heated lines maintained at 40 °C, which effectively suppressed rapid temperature fluctuations. The CIMS directly reports wet mole fractions (ppbv) for OOMs and HNO_3, while dry mole fraction is conventionally used in flux calculation. To assess the bias associated with using wet mole fraction and wet air density, 1-Hz CIMS inlet air temperature (T_a) and RH were interpolated to 10 Hz to compute dry mole fractions. This interpolation is valid because atmospheric water vapor content is only 0.5–2% by volume, so high-frequency water vapor fluctuations have negligible impact on HNO_3 and OOM dry mole fraction fluctuations. Water vapor mole fraction was calculated using Tetens' equation (Bolton, 1980): $RH \times 6.112 \exp\left(\frac{17.67T_a}{T_a+243.5}\right)/P$, where P is atmospheric pressure (hPa) measured at the supersite. Fluxes were then recalculated using dry mole fraction and dry air density (dry formulation) and compared with those using wet mole fraction and wet air density (wet formulation).

Fluxes from wet and dry formulations agree closely for all species ($R^2 \geq 0.97$, Figure S7). Wet-formulation fluxes are ~1.1% higher for HNO_3 (slope = 1.0108), ~1.2% higher for $C_4H_7NO_5$ (slope = 1.0122), and ~1.3% lower for CH_2O_2 (slope = 0.9871). Overall,

https://doi.org/10.5194/egusphere-2026-3089
Preprint. Discussion started: 11 June 2026

water vapor-induced bias is within ± 2% for all species, much smaller than the system's total flux uncertainty (Table 1) and thus negligible. All fluxes reported herein use measured wet mole fraction and wet air density.

3.3 Flux analysis

In total, we observed 16 OOM species (including 12 CHO-OOMs and 4 CHON-OOMs) with detectable fluxes during the summer campaign. Time series of concentrations and fluxes of the 4 selected species (HNO_3, $C_4H_7NO_5$, CH_2O_2, and $C_3H_4O_4$) are provided in Figure S6. Diurnal peak mixing ratios of the medium-SNR OOMs $C_4H_7NO_5$ and CH_2O_2 were 0.216 ± 0.031 and 0.069 ± 0.010 ppbv, respectively. Their downward flux detection rates are 22.5% and 12.6% of all 30-min intervals, with corresponding mean peak downward fluxes of -0.051 and -0.023 nmol m^{-2} s^{-1} (Table 1). Their upward flux detection rates were lower, ranging from 1.4% to 5.3% of all 30-min intervals.

The fluxes observed in this urban location are much lower than those forest canopy-atmosphere fluxes (Fulgham et al., 2019; Nguyen et al., 2015; Vermeuel et al., 2023). For example, formic acid peak fluxes above forests were around 1-2 nmol m^{-2} s^{-1}, either emission or deposition, with mean peak mixing ratio around 2.5 ppbv. Mean peak total fluxes of full-spectrum OOMs detected by I-CIMS were around 2.5 nmol carbon m^{-2} s^{-1} (both emission and deposition) over a coniferous forest (Vermeuel et al., 2023), much higher than 0.30 nmol carbon m^{-2} s^{-1} downward flux and 0.17 nmol carbon m^{-2} s^{-1} upward flux of total 16 OOM species in our study.

Based on the direction and magnitude of fluxes, observation days were classified into three categories: positive-flux days, negative-flux days, and no/weak-flux days. Mean diurnal variations of fluxes on these three categories of days are presented in Figure 2 for the 16 OOM species. Below we examine OOM flux directions, magnitudes, and their dependences on mixing ratios (Figure 3) and key meteorological parameters (u^*, z/L, temperature, solar radiation, shown in Figure S8-S11).

3.3.1 CHO-OOMs

Based on flux directions (Figure 2), the 12 CHO-OOMs are classified into three

https://doi.org/10.5194/egusphere-2026-3089
Preprint. Discussion started: 11 June 2026

groups: deposition-dominated, emission-dominated, and bidirectional OOM, indicating complex source-sink dynamics over urban surfaces. Six deposition-dominated OOMs ($C_3H_6O_3$, $C_4H_8O_4$, $C_5H_6O_4$, $C_5H_8O_4$, $C_5H_{10}O_3$, $C_9H_8O_2$) showed negative fluxes on 14 - 40% of observation days, with mean diurnal peak values of -4.26, -8.50, -3.26, -5.32, -11.4, and -2.85 pmol m^{-2} s^{-1}, respectively. This indicates deposition exceeded near-surface emissions and chemical production on these days, making urban surfaces a net sink for these species.

Mixing ratios of these six species were significantly higher on negative-flux days than on no/weak-flux days (Figure 3). Elevated concentrations appearing to be the direct driver of the observed negative fluxes. No statistically significant differences in key turbulence parameters (u*, z/L) were observed between the two categories of days (Figures S8 and S9). However, deposition flux diurnal variations were modulated by turbulence: maximum fluxes for all six OOMs consistently occurred between 12:00–16:00 when turbulence was most fully developed, rather than peak concentration hours. As widely documented in previous I-CIMS studies, these species are inferred to be isoprene oxidation products (2-methylglyceric acid $C_4H_8O_4$; IEPOX+ISOPOOH $C_5H_{10}O_3$), glutaric acid $C_5H_8O_4$ and lactic acid $C_3H_6O_3$ formed from oxidation of anthropogenic and biogenic precursors, citraconic acid $C_5H_6O_4$ and trans-cinnamic acid $C_9H_8O_2$ from biomass burning (Oghama et al., 2025).

The second group, comprising $C_5H_{10}O_4$, $C_5H_{12}O_4$, $C_7H_{10}O_4$, and $C_7H_{12}O_4$, exhibited positive fluxes on 11–32% of observation days, with mean diurnal peak values of 5.88, 5.39, 3.38, and 2.96 pmol m^{-2} s^{-1}, respectively. On positive-flux days, these species showed enhanced daytime emissions and elevated concentrations, coinciding with higher temperature and solar radiation than no/weak-flux days (Figures S10 and S11). These OOMs likely originate from direct surface emissions or form via rapid near-surface photooxidation of precursors. The resulting upward concentration gradient gives rise to the observed apparent positive fluxes. $C_5H_{12}O_4$ is 2-methyltetrols from isoprene oxidation. $C_5H_{10}O_4$ is an isoprene oxidation product but also found in food cooking emission (Ernesto et al., 2018; Mehra et al., 2021). Saturated dicarboxylic acid

https://doi.org/10.5194/egusphere-2026-3089
Preprint. Discussion started: 11 June 2026

$C_7H_{12}O_4$ may be from thermally enhanced vegetation emission or biomass burning (Kawamura and Bikkina, 2016). $C_7H_{10}O_4$ is of secondary origin from toluene oxidation (Wang et al., 2020).

The third group, comprising CH_2O_2 (formic acid) and $C_2H_4O_3$ (peracetic acid), exhibited bidirectional flux patterns. Formic acid and peracetic acid have various primary emission sources and secondary photochemical origins, so their bidirectional fluxes reflect competition between atmospheric deposition and near-surface emissions plus chemical production. In fact, no/weak-flux days accounted for 50% and 57% of the observation days for the two OOMs. We attribute these weak/undetectable fluxes to values below the EC flux detection limit, not an absence of surface exchange processes.

3.2.2 CHON-OOMs

CHON-OOMs comprised two acyl peroxy nitrates (PAN: $C_2H_3NO_5$; PPN: $C_3H_5NO_5$), one isoprene-derived organonitrate ($C_4H_7NO_5$), and one nitrophenol ($C_6H_5NO_3$). Both acyl peroxy nitrates form from acyl peroxy radicals + NO_2: PAN from anthropogenic or biogenic VOC oxidation, PPN from anthropogenic n-alkanes (Min et al., 2012; Phillips et al., 2013; Turnipseed et al., 2006; Wolfe et al., 2009). $C_4H_7NO_5$, often assigned to methacrolein and methyl vinyl ketone hydroxy nitrate (MACN/MVKN), are multi-generational oxidation products of isoprene in NO_x-influenced regions (Mayhew et al., 2022; Tsiligiannis et al., 2022). Nitrophenol ($C_6H_5NO_3$) is anthropogenic, originating from primary combustion/industrial emissions and secondary oxidation of phenolics with NO_x.

Positive fluxes of PAN and nitrophenol were detected on 14% and 21% of the observation days, with corresponding diurnal flux peaks of 4.86, and 8.49 pmol m^{-2} s^{-1}, respectively; higher mean radiation was observed on these positive-flux days (Figure S11). Negative fluxes of PPN and MACN/MVKN were observed on 25% and 50% of the observation days, with their diurnal flux peaks on negative-flux days reaching -5.16 and -37.3 pmol m^{-2} s^{-1}, respectively. Although the four species exhibited unimodal or bimodal concentration patterns (Figure 3), their flux maxima all occurred during the daytime with fully developed turbulence.

https://doi.org/10.5194/egusphere-2026-3089
Preprint. Discussion started: 11 June 2026

3.3.3 Summer campaign-averaged OOMs fluxes and comparison with HNO_3

Given the complex flux behavior of OOMs, we aggregated all positive and negative fluxes separately for the entire summer campaign and calculated campaign-averaged daily values for each species (Figure 4a). Campaign-averaged daily negative flux of the 16 OOM species was 1.64 μmol m^{-2} d^{-1}, with CHON-OOMs contributing 59.4% and CHO-OOMs contributing the remaining 40.6%. The top three contributors to the total negative flux were the isoprene-derived MACN/MVKN ($C_4H_7NO_5$), the sum of IEPOX and ISOPOOH ($C_5H_{10}O_3$), and formic acid, collectively accounting for 79% of the total OOM negative flux.

Total campaign-averaged daily positive flux of OOMs was 0.41 μmol m^{-2} d^{-1}, equal to 25% of the total negative flux. CHON-OOMs contributed 33% of the total positive flux, while CHO-OOMs accounted for 67%. The top three contributors to the positive flux were formic acid, nitrophenol $C_6H_5NO_3$, and toluene-derived $C_7H_{10}O_4$, accounting for 63% of the total OOM positive flux.

For comparison, total campaign-averaged daily negative flux of all OOMs accounted for only 16.3% of that of nitric acid, which showed downward flux in 70.0% of all 30-min intervals (Table 1) and in 18 of 28 observation days (Figure S6). As a deposition-dominated species, HNO_3 mean diurnal flux on negative-flux days was unimodal, peaking at -0.59 nmol m^{-2} s^{-1} at 14:00 local time (Figure 4b). This HNO_3 peak was one to two orders of magnitude larger than the OOM flux peaks on negative-flux days, but was closer to mean HNO_3 peak fluxes of -2.636 and -0.558 nmol m^{-2} s^{-1} reported over forest canopies (Horii et al., 2006; Nguyen et al., 2015). In terms of mixing ratio, mean diurnal peaks of HNO_3 (0.414 ± 0.266ppbv) and $C_4H_7NO_5$ (0.216 ± 0.031) were one order of magnitude higher than other OOMs (tens of pptv. Figure 3).

4. Conclusion

This is the first direct eddy covariance flux measurement of pptv-level OOMs in an urban environment. While urban environments are generally recognized as having more severe anthropogenic organic pollution, the OOM fluxes measured at this urban site

https://doi.org/10.5194/egusphere-2026-3089
Preprint. Discussion started: 11 June 2026

were one to two orders of magnitude lower than those reported in previous observations above forest canopies. This discrepancy likely stems from the fact that forest canopy flux measurements are taken directly a few meters above biogenic emission sources, whereas our study was conducted at a suburban university campus distant from downtown areas, industrial zones, and traffic emission sources. Accordingly, we optimized the flux processing workflow for low-SNR OOMs, including noise subtraction from power spectra, compound-specific spectral correction using the empirical Ibrom method, and uniform lag time determination using high-SNR HNO_3 as a reference tracer. We also systematically investigated the effects of data block averaging and water vapor dilution on flux estimates.

Our flux observation of HNO_3 and 16 OOM species reveals complex bidirectional exchange shaped by competing biogenic/anthropogenic emissions, near-surface photochemistry, and dry deposition. The campaign-averaged total daily OOM deposition flux (1.64 μmol m^{-2} d^{-1}) was four times larger than the total daily emission flux (0.41 μmol m^{-2} d^{-1}). Isoprene-derived organonitrate $C_4H_7NO_5$, IEPOX+ISOPOOH ($C_5H_{10}O_3$), formic acid (CH_2O_2), and nitrophenol $C_6H_5NO_3$ were identified as the dominant contributors to the total OOM fluxes.

This work fills a critical gap in urban atmospheric chemistry observations by providing a comprehensive dataset of full-spectrum OOM surface-atmosphere fluxes. The results offer essential observational constraints for chemical transport models, which currently lack accurate parameterizations for OOM dry deposition due to limited field measurements. We acknowledge that short-term measurements are insufficient to quantify these individual processes and their drivers. Nevertheless, this work establishes the foundation for future study and underscores the necessity of combining long-term flux observations with advanced modeling to fully elucidate the source and sink of OOMs in urban atmosphere.

Data availability. The data used in this article are available from the public data repository Zenodo at https://doi.org/10.5281/zenodo.20437228 (Yu et al. 2026)

https://doi.org/10.5194/egusphere-2026-3089
Preprint. Discussion started: 11 June 2026

Acknowledgments

This research was supported by the National Key Research and Development Program of China (grant no. 2023YFC3709801), the National Natural Science Foundation of China (grant no. 42175131), and the Fundamental Research Funds (grant no. G1323523063) for the Central Universities, China University of Geosciences (Wuhan).

Competing interests

The contact author has declared that none of the authors has any competing interests.

Author contributions.

HY designed the study. JS, XW, and HY built and characterized the system. JH, XW, JH, BZ, and NC contributed to field measurement. JS, XW and HY analyzed the data and wrote the manuscript.

https://doi.org/10.5194/egusphere-2026-3089
Preprint. Discussion started: 11 June 2026

Figures and table

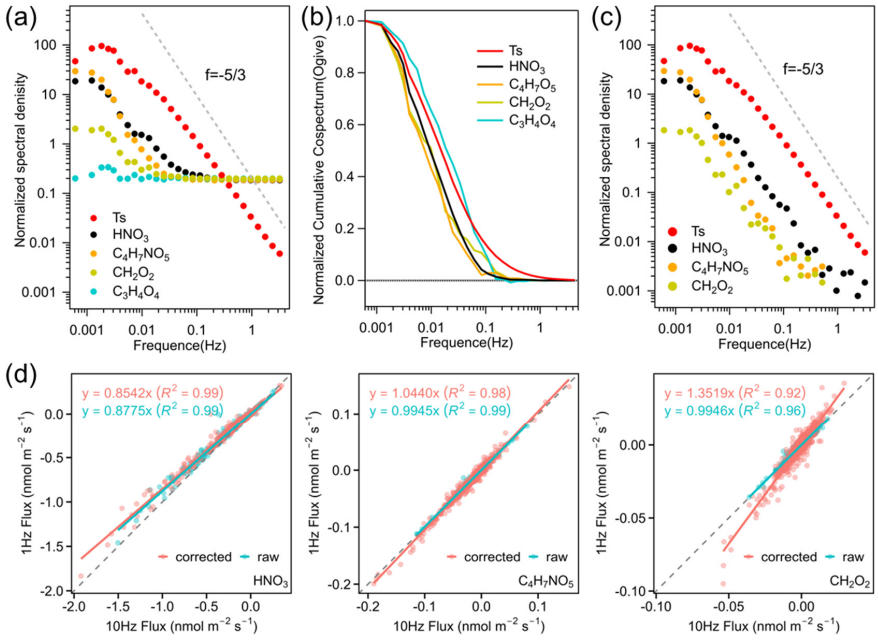

Figure 1. Spectral characteristics of sonic temperature (T_s) and selected species (HNO_3, $C_4H_7NO_5$, CH_2O_2, $C_3H_4O_4$) with varying SNRs, for all 30-minute intervals (12:00–15:00) during the campaign: **(a)** mean normalized power spectra; **(b)** mean normalized cumulative cospectra (ogives) with vertical wind velocity; **(c)** denoised mean normalized power spectra. Gray dashed lines denote the theoretical Kolmogorov −5/3 slope. **(d)** Correlations between 1 Hz and 10 Hz fluxes for HNO_3, $C_4H_7NO_5$ and CH_2O_2: raw fluxes (blue) and spectrally corrected fluxes (red). The gray dashed line indicating y=x.

https://doi.org/10.5194/egusphere-2026-3089
Preprint. Discussion started: 11 June 2026

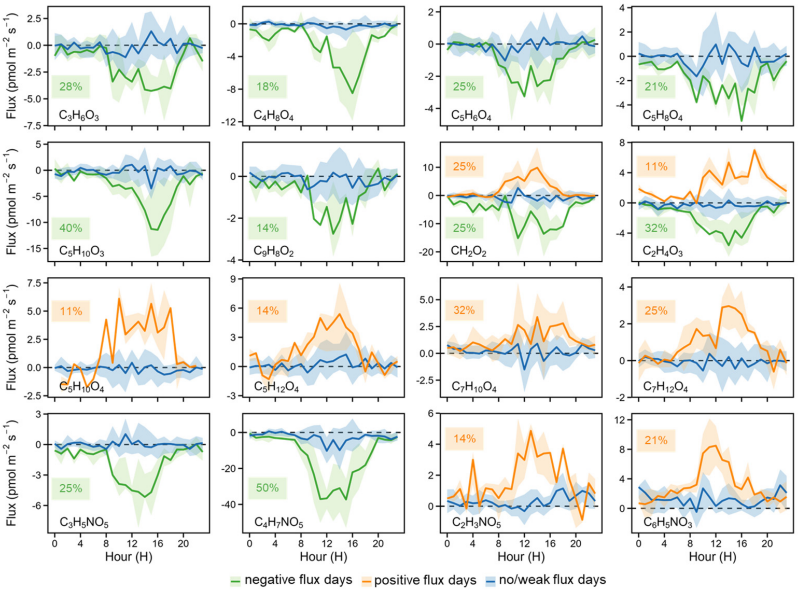

Figure 2. Diurnal cycles of OOM fluxes, grouped by flux sign: positive (orange), negative (green), and no/weak flux (blue) days. Percentages denote the fractions of positive and negative flux days relative to all observation days; shaded areas mark 25th - 75th percentiles.

https://doi.org/10.5194/egusphere-2026-3089
Preprint. Discussion started: 11 June 2026

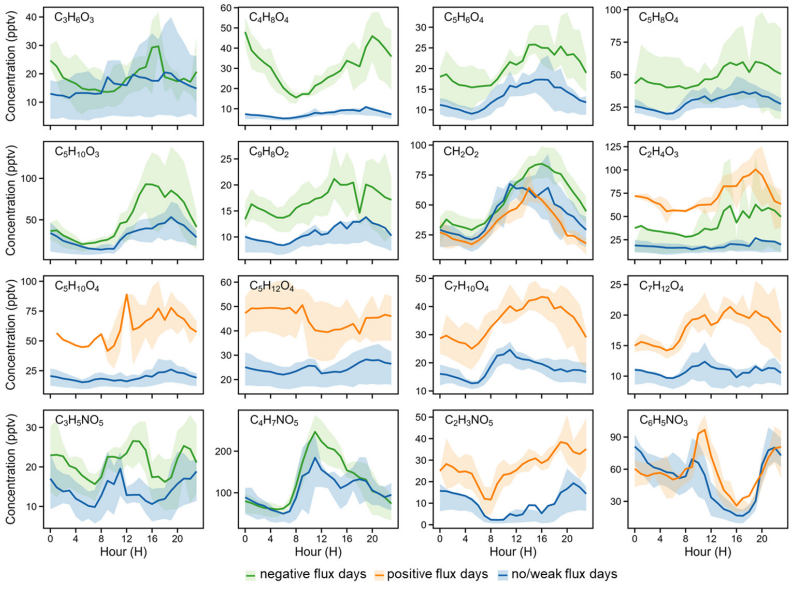

Figure 3. Diurnal cycles of OOMs mixing ratios grouped by flux sign: positive (orange), negative (green), and no/weak flux (blue) days. Shaded areas represent the corresponding 25th and 75th percentiles.

https://doi.org/10.5194/egusphere-2026-3089
Preprint. Discussion started: 11 June 2026

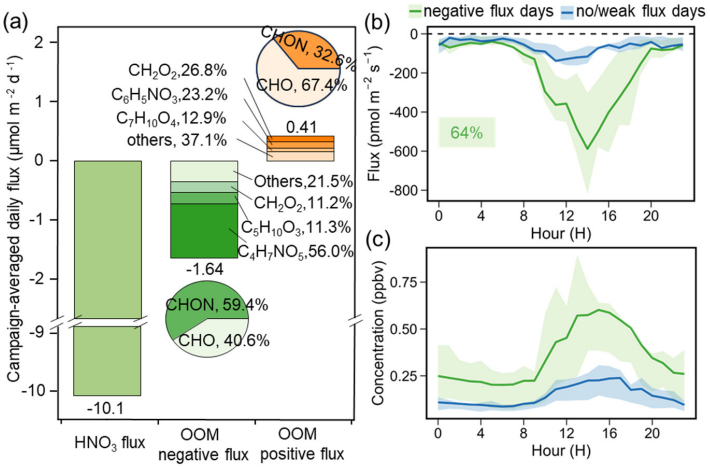

Figure 4. (a) Campaign-averaged daily fluxes (including species contributions). Diurnal cycles of HNO_3: **(b)** fluxes and **(c)** mixing ratios, grouped by flux sign: negative (green), and no/weak flux days (blue). Percentages denote the fractions of negative flux days relative to all observation days. Shaded areas represent the corresponding 25th and 75th percentiles.

https://doi.org/10.5194/egusphere-2026-3089
Preprint. Discussion started: 11 June 2026

Table 1. Spectral correction factors, spectral flux losses, mean detection limits (DL), mean sampling random uncertainties, detection rates in all 30-min intervals, and mean peak fluxes for HNO_3 and selected OOMs. Random sampling uncertainty is defined as the mean σ_F/F for all 30-min fluxes above DL.

	HNO_3	$C_4H_7NO_5$	CH_2O_2
LPSCF (mean ± sd)	1.12 ± 0.05	1.49 ± 0.23	1.22 ± 0.11
High-frequency flux loss (mean ± sd)	10.9% ± 3.9%	31.5% ± 9.8%	17.6% ± 6.6%
SCF(mean ± sd)	1.27 ± 0.05	1.78 ± 0.22	1.53 ± 0.12
total spectral flux loss (mean ± sd)	21.1% ± 2.8%	42.9% ± 6.5%	34.1% ± 4.8%
Mean sampling random uncertainty (%)	±29.88%	±36.39%	±37.92%
Mean detection limit (nmol m^{-2} s^{-1})	0.75×10^{-2}	0.52×10^{-2}	2.12×10^{-3}
Detection rate of upward fluxes (%)	0.43%	1.39%	5.34%
Mean peak upward fluxes above DL (nmol m^{-2} s^{-1})	/	3.60×10^{-2}	1.69×10^{-2}
Detection rate of downward fluxes (%)	69.98%	22.50%	12.61%
Mean peak downward fluxes above DL(nmol m^{-2} s^{-1})	-7.44×10^{-1}	-5.08×10^{-2}	-2.25×10^{-2}

https://doi.org/10.5194/egusphere-2026-3089
Preprint. Discussion started: 11 June 2026

Reference

Acton, W. J. F., Huang, Z., Davison, B., Drysdale, W. S., Fu, P., Hollaway, M., Langford, B., Lee, J., Liu, Y., & Metzger, S. (2020). Surface–atmosphere fluxes of volatile organic compounds in Beijing. *Atmospheric Chemistry and Physics*, *20(23)*, 1-36. https://doi.org/10.5194/acp-20-15101-2020

Bachy, A., Aubinet, M., Amelynck, C., Schoon, N., Bodson, B., Delaplace, P., De Ligne, A., Digrado, A., du Jardin, P., & Fauconnier, M.-L. (2020). Dynamics and mechanisms of volatile organic compound exchanges in a winter wheat field. *Atmospheric Environment*, *221(15)*, 117105. https://doi.org/10.1016/j.atmosenv.2019.117105

Beaver, M. R., Clair, J. M. S., Paulot, F., Spencer, K. M., Crounse, J. D., LaFranchi, B. W., Min, K. E., Pusede, S. E., Wooldridge, P. J., & Schade, G. W. (2012). Importance of biogenic precursors to the budget of organic nitrates: observations of multifunctional organic nitrates by CIMS and TD-LIF during BEARPEX 2009. *Atmospheric Chemistry and Physics*, *12(13)*, 5773-5785. https://doi.org/10.5194/acp-12-5773-2012

Bertram, T., Kimmel, J., Crisp, T., Ryder, O., Yatavelli, R., Thornton, J., Cubison, M., Gonin, M., & Worsnop, D. (2011). A field-deployable, chemical ionization time-of-flight mass spectrometer. *Atmospheric Measurement Techniques*, *4(7)*, 1471-1479. https://doi.org/10.5194/amt-4-1471-2011

Bolton, D. (1980). The computation of equivalent potential temperature. *Monthly Weather Review*, *108(7)*, 1046-1053. https://doi.org/10.1175/1520-0493(1980)108.

Coggon, M. M., Gkatzelis, G. I., McDonald, B. C., Gilman, J. B., Schwantes, R. H., Abuhassan, N., Aikin, K. C., Arend, M. F., Berkoff, T. A., & Brown, S. S. (2021). Volatile chemical product emissions enhance ozone and modulate urban chemistry. *Proceedings of the National Academy of Sciences*, *118(32)*, e2026653118. https://doi.org/10.1073/pnas.2026653118

DiGangi, J. P., Boyle, E. S., Karl, T., Harley, P., Turnipseed, A., Kim, S., Cantrell, C., Maudlin Iii, R. L., Zheng, W., & Flocke, F. (2011). First direct measurements of formaldehyde flux via eddy covariance: implications for missing in-canopy

https://doi.org/10.5194/egusphere-2026-3089
Preprint. Discussion started: 11 June 2026

formaldehyde sources. *Atmospheric Chemistry and Physics*, *11(20)*, 10565-10578. https://doi.org/10.5194/acp-11-10565-2011

Ehn, M., Thornton, J. A., Kleist, E., Sipilä, M., Junninen, H., Pullinen, I., Springer, M., Rubach, F., Tillmann, R., & Lee, B. (2014). A large source of low-volatility secondary organic aerosol. *Nature*, *506(7489)*, 476-479. https://doi.org/10.1038/nature13032

Ernesto, R. V., Michael, L. B., Archit, M., Michael, P., Carl, P., Hugh, C., & James D, A. (2018). Online chemical characterization of food-cooking organic aerosols: Implications for source apportionment. *Environmental Science & Technology*, *52(9)*, 5308-5318. https://doi.org/10.1021/acs.est.7b06278

Fares, S., Park, J. H., Gentner, D. R., Weber, R., Ormeño, E., Karlik, J., & Goldstein, A. H. (2012). Seasonal cycles of biogenic volatile organic compound fluxes and concentrations in a California citrus orchard. *Atmospheric Chemistry and Physics*, *12(20)*, 9865-9880. https://doi.org/10.5194/acp-12-9865-2012

Finkelstein, P. L., & Sims, P. F. (2001). Sampling error in eddy correlation flux measurements. *Journal of Geophysical Research: Atmospheres*, *106(D4)*, 3503-3509. https://doi.org/10.1029/2000JD900731

Fischer, L., Breitenlechner, M., Canaval, E., Scholz, W., Striednig, M., Graus, M., Karl, T. G., Petäjä, T., Kulmala, M., & Hansel, A. (2021). First eddy covariance flux measurements of semi-volatile organic compounds with the PTR3-TOF-MS. *Atmospheric Measurement Techniques*, *14(12)*, 8019-8039. https://doi.org/10.5194/amt-14-8019-2021

Foken, T., Göockede, M., Mauder, M., Mahrt, L., Amiro, B., & Munger, W. (2004). Post-field data quality control, In X. Lee, W. Massman & B. Law (Eds.), *Handbook of micrometeorology: A guide for surface flux measurement and analysis*, *Atmospheric and Oceanographic Sciences Library* (Vol. 29, pp. 181-208). Springer, Dordrecht.

Fulgham, S. R., Brophy, P., Link, M., Ortega, J., Pollack, I., & Farmer, D. K. (2019). Seasonal flux measurements over a Colorado pine forest demonstrate a persistent

https://doi.org/10.5194/egusphere-2026-3089
Preprint. Discussion started: 11 June 2026

source of organic acids. *ACS Earth and Space Chemistry*, *3(9)*, 2017-2032. https://doi.org/10.1021/acsearthspacechem.9b00182

Gao, Z., Vasilakos, P., Nah, T., Takeuchi, M., Chen, H., Tanner, D. J., Ng, N. L., Kaiser, J., Huey, L. G., & Weber, R. J. (2022). Emissions, chemistry or bidirectional surface transfer? Gas phase formic acid dynamics in the atmosphere. *Atmospheric Environment*, *274*, 118995. https://doi.org/10.1016/j.atmosenv.2022.118995

He, X., Yuan, B., Huangfu, Y., Wang, S., Chen, Y., Zhang, X., Sun, Y., Karl, T., & Shao, M. (2026). Comprehensive characterization and source analysis of VOC fluxes in a Chinese megacity. *Environmental Science & Technology*, *60(8)*, 6477-6488. https://doi.org/10.1021/acs.est.5c16873

Hodzic, A., Madronich, S., Aumont, B., Lee-Taylor, J., Karl, T., Camredon, M., & Mouchel-Vallon, C. (2013). Limited influence of dry deposition of semivolatile organic vapors on secondary organic aerosol formation in the urban plume. *Geophysical Research Letters*, *40(12)*, 3302-3307. https://doi.org/10.1002/grl.50611

Horii, C. V., Munger, J. W., Wofsy, S. C., Zahniser, M., Nelson, D., & McManus, J. B. (2006). Atmospheric reactive nitrogen concentration and flux budgets at a Northeastern US forest site. *Agricultural And Forest Meteorology*, *136(3-4)*, 159-174. https://doi.org/10.1016/j.agrformet.2006.03.005

Hörtnagl, L., Bamberger, I., Graus, M., Ruuskanen, T. M., Schnitzhofer, R., Müller, M., Hansel, A., & Wohlfahrt, G. (2011). Biotic, abiotic, and management controls on methanol exchange above a temperate mountain grassland. *Journal of Geophysical Research: Biogeosciences*, *116(G3)*. https://doi.org/10.1029/2011JG001641

Ibrom, A., Dellwik, E., Flyvbjerg, H., Jensen, N. O., & Pilegaard, K. (2007). Strong low-pass filtering effects on water vapour flux measurements with closed-path eddy correlation systems. *Agricultural And Forest Meteorology*, *147(3-4)*, 140-156. https://doi.org/10.1016/j.agrformet.2007.07.007

Isaacman-VanWertz, G., Massoli, P., O'Brien, R., Lim, C., Franklin, J. P., Moss, J. A., Hunter, J. F., Nowak, J. B., Canagaratna, M. R., & Misztal, P. K. (2018). Chemical evolution of atmospheric organic carbon over multiple generations of oxidation.

https://doi.org/10.5194/egusphere-2026-3089
Preprint. Discussion started: 11 June 2026

Nature Chemistry, *10(4)*, 462-468. https://doi.org/10.1038/s41557-018-0002-2

Karl, T., Striednig, M., Graus, M., Hammerle, A. and Wohlfahrt, G. (2018). Urban flux measurements reveal a large pool of oxygenated volatile organic compound emissions. Proceedings of the National Academy of Sciences, 115 (6): 1186-1191. https://doi: 10.1073/pnas.1714715115

Kawamura, K., & Bikkina, S. (2016). A review of dicarboxylic acids and related compounds in atmospheric aerosols: Molecular distributions, sources and transformation. *Atmospheric Research*, *170*, 140-160. https://doi.org/10.1016/j.atmosres.2015.11.018

Kelly, J. M., Doherty, R. M., O'Connor, F. M., Mann, G. W., Coe, H., & Liu, D. (2019). The roles of volatile organic compound deposition and oxidation mechanisms in determining secondary organic aerosol production: a global perspective using the UKCA chemistry–climate model (vn8. 4). *Geoscientific Model Development*, *12(6)*, 2539-2569. https://doi.org/10.5194/gmd-12-2539-2019

Kim, M. J., Novak, G. A., Zoerb, M. C., Yang, M., Blomquist, B. W., Huebert, B. J., Cappa, C. D., & Bertram, T. H. (2017). Air-sea exchange of biogenic volatile organic compounds and the impact on aerosol particle size distributions. *Geophysical Research Letters*, *44(8)*, 3887-3896. https://doi.org/10.1002/2017GL072975

Langford, B., Acton, W., Ammann, C., Valach, A., & Nemitz, E. (2015). Eddy-covariance data with low signal-to-noise ratio: time-lag determination, uncertainties and limit of detection. *Atmospheric Measurement Techniques*, *8(10)*, 4197-4213. https://doi.org/10.5194/amt-8-4197-2015

Lee, B. H., Lopez-Hilfiker, F. D., Mohr, C., Kurtén, T., Worsnop, D. R., & Thornton, J. A. (2014). An iodide-adduct high-resolution time-of-flight chemical-ionization mass spectrometer: Application to atmospheric inorganic and organic compounds. *Environmental Science & Technology*, *48(11)*, 6309-6317. https://doi.org/10.1021/es500362a

Liu, X., Deming, B., Pagonis, D., Day, D. A., Palm, B. B., Talukdar, R., Roberts, J. M., Veres, P. R., Krechmer, J. E., & Thornton, J. A. (2019). Effects of gas–wall

https://doi.org/10.5194/egusphere-2026-3089
Preprint. Discussion started: 11 June 2026

interactions on measurements of semivolatile compounds and small polar molecules. *Atmospheric Measurement Techniques*, *12(6)*, 3137-3149. https://doi.org/10.5194/amt-12-3137-2019

Lopez-Hilfiker, F. D., Iyer, S., Mohr, C., Lee, B. H., D'Ambro, E. L., Kurtén, T., & Thornton, J. A. (2016). Constraining the sensitivity of iodide adduct chemical ionization mass spectrometry to multifunctional organic molecules using the collision limit and thermodynamic stability of iodide ion adducts. *Atmospheric Measurement Techniques*, *9(4)*, 1505-1512. https://doi.org/10.5194/amt-9-1505-2016

Manco, A., Ciccioli, P., Famulari, D., Brilli, F., Ciccioli, P., Di Tommasi, P., Toscano, P., Gioli, B., Esposito, A., & Magliulo, V. (2022). Real-time air concentrations and turbulent fluxes of volatile organic compounds (VOCs) over historic closed landfills to assess their potential environmental impact. *Environmental Pollution*, *309*, 119748. https://doi.org/10.1016/j.envpol.2022.119748

Mattila, J. M., Brophy, P., Kirkland, J., Hall, S., Ullmann, K., Fischer, E. V., Brown, S., McDuffie, E., Tevlin, A., & Farmer, D. K. (2018). Tropospheric sources and sinks of gas-phase acids in the Colorado Front Range. *Atmospheric Chemistry and Physics*, *18(16)*, 12315-12327. https://doi.org/10.5194/acp-18-12315-2018

Mayhew, A. W., Lee, B. H., Thornton, J. A., Bannan, T. J., Brean, J., Hopkins, J. R., Lee, J. D., Nelson, B. S., Percival, C., & Rickard, A. R. (2022). Evaluation of isoprene nitrate chemistry in detailed chemical mechanisms. *Atmospheric Chemistry and Physics*, *22(22)*, 14783-14798. https://doi.org/10.5194/acp-22-14783-2022

Mehra, A., Canagaratna, M., Bannan, T. J., Worrall, S. D., Bacak, A., Priestley, M., Liu, D., Zhao, J., Xu, W., & Sun, Y. (2021). Using highly time-resolved online mass spectrometry to examine biogenic and anthropogenic contributions to organic aerosol in Beijing. *Faraday Discussions*, *226*, 382-408. https://doi.org/10.1039/D0FD00080A

Min, K.-E., Pusede, S., Browne, E., LaFranchi, B., Wooldridge, P., Wolfe, G., Harrold, S., Thornton, J., & Cohen, R. (2012). Observations of atmosphere-biosphere

https://doi.org/10.5194/egusphere-2026-3089
Preprint. Discussion started: 11 June 2026

exchange of total and speciated peroxynitrates: nitrogen fluxes and biogenic sources of peroxynitrates. *Atmospheric Chemistry and Physics*, *12(20)*, 9763-9773. https://doi.org/10.5194/acp-12-9763-2012

Moncrieff, J., Clement, R., Finnigan, J., & Meyers, T. (2004). Averaging, detrending, and filtering of eddy covariance time series, In X. Lee, W. Massman & B. Law (Eds.), *Handbook of micrometeorology: A guide for surface flux measurement and analysis*, *Atmospheric and Oceanographic Sciences Library* (Vol. 29, pp. 7-31). Springer, Dordrecht.

Moncrieff, J. B., Massheder, J. M., De Bruin, H., Elbers, J., Friborg, T., Heusinkveld, B., Kabat, P., Scott, S., Soegaard, H., & Verhoef, A. (1997). A system to measure surface fluxes of momentum, sensible heat, water vapour and carbon dioxide. *Journal of Hydrology*, *188-189*, 589-611. https://doi.org/10.1016/S0022-1694(96)03194-0

Nguyen, T. B., Crounse, J. D., Teng, A. P., St. Clair, J. M., Paulot, F., Wolfe, G. M., & Wennberg, P. O. (2015). Rapid deposition of oxidized biogenic compounds to a temperate forest. *Proceedings of the National Academy of Sciences of the United States of America*, *112(5)*, E392-E401. https://doi.org/10.1073/pnas.1418702112

Oghama, O. E., Voliotis, A., Bannan, T. J., Syafira, S. A., Hu, D., Wu, H., Gallimore, P., McFiggans, G., Coe, H., & Allan, J. D. (2025). Variations in oxygenated and nitrogen-containing primary organic compounds based on the fuel type and burning condition in stove emissions. *Environmental Science: Atmospheres*, *5(12)*, 1297-1311. https://doi.org/10.1039/D5EA00080G

Phillips, G. J., Pouvesle, N., Thieser, J., Schuster, G., Axinte, R., Fischer, H., Williams, J., Lelieveld, J., & Crowley, J. N. (2013). Peroxyacetyl nitrate (PAN) and peroxyacetic acid (PAA) measurements by iodide chemical ionisation mass spectrometry: first analysis of results in the boreal forest and implications for the measurement of PAN fluxes. *Atmospheric Chemistry and Physics*, *13(3)*, 1129-1139. https://doi.org/10.5194/acp-13-1129-2013

Ruuskanen, T. M., Müller, M., Schnitzhofer, R., Karl, T., Graus, M., Bamberger, I.,

https://doi.org/10.5194/egusphere-2026-3089
Preprint. Discussion started: 11 June 2026

Hörtnagl, L., Brilli, F., Wohlfahrt, G., & Hansel, A. (2011). Eddy covariance VOC emission and deposition fluxes above grassland using PTR-TOF. *Atmospheric Chemistry and Physics*, *11(2)*, 611-625. https://doi.org/10.5194/acp-11-611-2011

Schobesberger, S., Lopez-Hilfiker, F. D., Taipale, D., Millet, D. B., D'Ambro, E. L., Rantala, P., Mammarella, I., Zhou, P., Wolfe, G. M., & Lee, B. H. (2016). High upward fluxes of formic acid from a boreal forest canopy. *Geophysical Research Letters*, *43(17)*, 9342-9351. https://doi.org/10.1002/2016GL069599

Tsiligiannis, E., Wu, R., Lee, B. H., Salvador, C. M., Priestley, M., Carlsson, P. T., Kang, S., Novelli, A., Vereecken, L., & Fuchs, H. (2022). A four carbon organonitrate as a significant product of secondary isoprene chemistry. *Geophysical Research Letters*, *49(11)*, e2021GL097366. https://doi.org/10.1029/2021GL097366

Turnipseed, A. A., Huey, L. G., Nemitz, E., Stickel, R., Higgs, J., Tanner, D. J., Slusher, D. L., Sparks, J. P., Flocke, F., & Guenther, A. (2006). Eddy covariance fluxes of peroxyacetyl nitrates (PANs) and NOy to a coniferous forest. *Journal of Geophysical Research: Atmospheres*, *111(D9)*. https://doi.org/10.1029/2005JD006631Digital

Valach, A. C., Langford, B., Nemitz, E., MacKenzie, A. R., & Hewitt, C. N. (2015). Seasonal and diurnal trends in concentrations and fluxes of volatile organic compounds in central London. *Atmospheric Chemistry and Physics*, *15(14)*, 7777-7796. https://doi.org/10.5194/acp-15-7777-2015

Velasco, E., Pressley, S., Grivicke, R., Allwine, E., Coons, T., Foster, W., Jobson, B. T., Westberg, H., Ramos, R., & Hernández, F. (2009). Eddy covariance flux measurements of pollutant gases in urban Mexico City. *Atmospheric Chemistry and Physics*, *9(19)*, 7325-7342. https://doi.org/10.5194/acp-9-7325-2009

Vermeuel, M. P., Millet, D. B., Farmer, D. K., Pothier, M. A., Link, M. F., Riches, M., Williams, S., & Garofalo, L. A. (2023). Closing the reactive carbon flux budget: Observations from dual mass spectrometers over a coniferous forest. *Journal of Geophysical Research: Atmospheres*, *128(14)*, e2023JD038753. https://doi.org/10.1029/2023JD038753

Vettikkat, L., Miettinen, P., Buchholz, A., Rantala, P., Yu, H., Schallhart, S., Petäjä, T.,

https://doi.org/10.5194/egusphere-2026-3089
Preprint. Discussion started: 11 June 2026

Seco, R., Männistö, E., Kulmala, M.,# Tuittila, E.-S., Guenther, A. B., and Schobesberger, S. (2023). High emission rates and strong temperature response make boreal wetlands a large source of isoprene and terpenes. *Atmospheric Chemistry and Physics*, *23(4)*, 2683-2698. https://doi.org/10.5194/acp-23-2683-2023

Vickers, D., & Mahrt, L. (1997). Quality control and flux sampling problems for tower and aircraft data. *Journal of Atmospheric and Oceanic Technology*, *14(3)*, 512-526. https://doi.org/10.1175/1520-0426(1997)014<0512:QCAFSP>2.0.CO;2

Wang, M., Chen, D., Xiao, M., Ye, Q., Stolzenburg, D., Hofbauer, V., Ye, P., Vogel, A. L., Mauldin III, R. L., & Amorim, A. (2020). Photo-oxidation of aromatic hydrocarbons produces low-volatility organic compounds. *Environmental science & technology*, *54(13)*, 7911-7921. https://doi.org/10.1021/acs.est.0c02100

Wolfe, G. M., Thornton, J. A., Yatavelli, R. L. N., McKay, M., Goldstein, A. H., LaFranchi, B., Min, K. E., & Cohen, R. C. (2009). Eddy covariance fluxes of acyl peroxy nitrates (PAN, PPN and MPAN) above a Ponderosa pine forest. *Atmospheric Chemistry and Physics*, *9(2)*, 615-634. https://doi.org/10.5194/acp-9-615-2009

Wu, Z., Zhang, L., Walker, J. T., Makar, P. A., Perlinger, J. A., & Wang, X. (2021). Extension of a gaseous dry deposition algorithm to oxidized volatile organic compounds and hydrogen cyanide for application in chemistry transport models. *Geoscientific Model Development*, *14(8)*, 5093-5105. https://doi.org/10.5194/gmd-14-5093-2021

Yang, M., Beale, R., Smyth, T., & Blomquist, B. (2013). Measurements of OVOC fluxes by eddy covariance using a proton-transfer-reaction mass spectrometer–method development at a coastal site. *Atmospheric Chemistry and Physics*, *13(13)*, 6165-6184. https://doi.org/10.5194/acp-13-6165-2013

Yu, H., Sun, J., & Wang, X. (2026). Eddy covariance data of urban surface-atmosphere fluxes of oxygenated organic molecules [Data set]. Zenodo. https://doi.org/10.5281/zenodo.20437228

Yuan, B., Kaser, L., Karl, T., Graus, M., Peischl, J., Campos, T. L., Shertz, S., Apel, E. C., Hornbrook, R. S., & Hills, A. (2015). Airborne flux measurements of methane

https://doi.org/10.5194/egusphere-2026-3089
Preprint. Discussion started: 11 June 2026

and volatile organic compounds over the Haynesville and Marcellus shale gas production regions. *Journal of Geophysical Research: Atmospheres*, *120(12)*, 6271-6289. https://doi.org/10.1002/2015JD023242

Zavarsky, A., Booge, D., Fiehn, A., Krüger, K., Atlas, E., & Marandino, C. (2018). The influence of air-sea fluxes on atmospheric aerosols during the summer monsoon over the tropical Indian Ocean. *Geophysical Research Letters*, *45(1)*, 418-426. https://doi.org/10.1002/2017GL076410

Zhang, L., Brook, J. R., & Vet, R. (2003). A revised parameterization for gaseous dry deposition in air-quality models. *Atmospheric Chemistry and Physics*, *3(6)*, 2067-2082. https://doi.org/10.5194/acp-3-2067-2003